Microstructure and properties of $FeCrMnNiC_x$ compositionally complex bulk alloys

Waleed Muftah and Vladimir Vishnyakov*

Surface Coating and Characterisation Research Group, Centre for Engineering Materials, University of Huddersfield, HD1 3DH, UK

Abstract

$FeCrMnNiC_x$ (x= 0.1, 0.3, 0.5 and 1) bulk alloys were synthesised by Vacuum Arc Smelting. The alloy with 2 at. % of carbon (x=0.1) is a single-phase and uniform material with no element or phase segregation. The alloys with higher carbon content were two phase materials. The equiatomic FeCrMnNiC alloy with two phases had the best corrosion resistance in 3.5% NaCl solution at room temperature under atmospheric pressure. Ion irradiation of $FeCrMnNiC_{0.1}$ with FCC structure by 600 KeV Xe^{+2} to 50 displacements per atom (dpa) at 623 K revealed the alloy high radiation hardness by the absence of phase transformation and elemental segregation. The single-phase $FeCrMnNiC_{0.1}$ alloy has a hardness of 7.5 ± 0.84 GPa and reduced Young's modulus of 250 ± 28.1 GPa.

Keywords

FeCrMnNiC high entropy compound material, compositionally complex alloy, single-phase alloy, corrosion resistance, radiation damage resistance, mechanical properties.

* Corresponding author: v.vishnyakov@hud.ac.uk, tel. +44 1484 472164

1. Introduction

In 2004, Yeh et al have announced new type of materials with multi-principal elements (e.g. elements in high concentration) composition known since then as High Entropy Alloys (HEAs) [1]. High entropy alloys were defined as multicomponent alloys containing five or more principle elements with equiatomic or near-equiatomic ratios. Many groups have deviated from this original definition and talk about HEAs which have many elements at concentration between 35 and 5 atomic percent (at. %) of each principle element [1, 2]. By and large, this is different from the conventional alloys which are based on a single dominant element such as; Cu-Zr [3, 4], Ni-Nb [5] binary bulk metallic glasses alloys and FeCrNi iron based ternary alloy [6]. High entropy (HE) term should, generally, only be used for alloys with equiatomic or near equiatomic atomic concentration ratio, and a single-phase microstructure [7]. It is evident that more accurate terms like compositionally complex alloys (CCAs) [8-10] and/or complex concentrated alloys (CCAs) [11-13] are more accurate in many cases. CCAs can have more than one phase and allow the elemental concentrations to be far from equal [11-13]. The number of elements also can be smaller than five. For instance, an alloy can be a ternary CoCrNi [14], and quaternary $CoFeNiSi_{0.5}$ [15]. CCAs forming multiphase microstructures might be more desirable for better mechanical properties rather than single phase microstructures which are known to limit the performance in engineering applications usage [16-22].

High entropy and compositionally complex alloys are produced out of combining many different metals such as: Fe, Cr, Co, Cu, Mg, Al and Ni [23]. The most used processing method to synthesise high entropy alloys or complex concentrated alloys is vacuum arc melting, which also can allow to reshape the smelted material in to ribbons, rods and bars [24]. Also, the smelting temperature can reach up to 3000 °C which is high enough to melt the majority of metals for producing HEAs or CCAs such as: $Al_{0.5}CoCrCuFeNi$ [25] and FeCoNiCrCu [26]. HEAs and CCAs showed good properties in many cases such as; high strength–ductility [27], high fracture resistance [28], excellent hardness and fracture toughness [29-31], high thermal stability [32], high oxidation resistance [33], and good wear resistance [34].

In terms of the corrosion performance, numerous types of HEAs and CCAs have been reported to exhibited good corrosion resistance in 3.5 wt. % (0.6 M NaCl) aqueous chloride solution. The good corrosion resistance alloys, for example, include: CoCrFeNi [35], $Fe_{38.5}Mn_{20}Co_{20}Cr_{15}Si_5Cu_{1.5}$ [36] and $Hf_{0.5}Nb_{0.5}Ta_{0.5}Ti_{1.5}Zr$ [37]. Furthermore, several studies have been carried out to investigate the effect of varying the element concentration on corrosion behaviour of HEAs and CCAs in different medias. Not all elements in high concentrations are beneficial or detrimental in all situations. For example a study showed that increasing Al content in $Al_xCoCrFeNi$ alloys led to decrease the corrosion resistance in a 0.6 M NaCl solution [38]. Also, the resistance of corrosion found to be reduced with an increasing of Al concentration in $Al_xCrFe_{1.5}MnNi_{0.5}$ alloys [39]. However, pitting corrosion improves with an increasing of Al content in each of the 0.5 M H_2SO4 and 1 M NaCl solutions [39]. Other elements like Mo in $Co_{1.5}CrFeNi_{1.5}Ti_{0.5}Mo_x$ enhance the pitting corrosion in 1 M NaCl solution [40]. In addition, a study of varying the composition concentration on AlCoFeNiTiZr alloys showed that due to the presence of dual phase the alloy had higher corrosion resistance [41]. In general, modifying a particular element concentration found to be beneficial in some alloys, and harmful in others.

Generally, the properties of a HEAs or CCAs can be improved by adding certain non-metallic elements such as O, B, N and C. The non-metallic additions allow to form complex oxides, borides, nitrides or carbides, these alloys called high entropy compound materials [42].

New generation of nuclear power stations will need materials with high radiation hardness. Many high entropy alloys were shown to be radiation resistant [43-48]. Nanocrystalline CoCuCrFeNi HEA synthesised by magnetron sputtering had shown phase stability under the MeV electron irradiation at 298 and 773 K [46]. However, there was a partial phase transformation from FCC to BCC at both temperatures at maximum dpa level (64 dpa) and grain growth was also observed at high temperature irradiation [46]. The irradiation of a $Fe_{27}Cr_{18}Mn_{27}Ni_{28}$ concentrated solid solution alloy with 3 and 5.8 MeV Ni ions in the temperature range from 673 to 973 K showed that the FCC phase did not exhibit any phase transformation up to doses around 10 dpa, but it was observed that radiation-induced segregation (RIS) at grain boundaries is significantly suppressed when compared to FeCrNi and FeMnCr conventional alloys [44].

Carbon is added to austenitic steels as the interstitial atoms could acquire exceptional mechanical properties due to creation of multiple structural changes such as complex compositions, reduction of grain size and triggering nano-twinning [49, 50]. The effect of adding a variant concentration of carbon on high entropy alloys have been investigated and showed to be beneficial to HEA properties. The hardness, strength and wear resistance of $CoCrFeNiC_x$ alloy have increased [51]. The oxidation resistance, scratch and hardness were improved of $FeCoCrNiW_{0.3}$+5 at.% of C alloy [52]. Hardness of FeCoCrNiMn with 2 at.% of C alloy was higher than carbon free alloy [53]. Irradiation resistant was enhanced in $Fe_{38}Mn_{40}Ni_{11}Al_4Cr_7C_x$ alloy [54]. Refractory alloys also enhanced by the presence of carbon in small concentrations [55].

An equiatomic quaternary FeCrMnNi alloy synthesised by arc melting furnace was found to have multi-phase alloy structure [56]. It was previously shown by us that equimolar thin film FeCrMnNiC is amorphous and has high hardness at around 12 GPa and has corrosion resistance better than 304 SS [57].

This work was aimed to find and characterise a novel single-phase bulk alloy. We report the synthesis and properties of new equiatomic and near equiatomic compositionally complex alloys - $FeCrMnNiC_x$ (x= 20, 10, 5 and 2 at%).

There are various ways to represent minor element in alloys. In this paper we have adopted the following representation: $FeCrMnNiC_x$ with 20 at% carbon is written as $FeCrMnNiC$; $FeCrMnNiC_x$ with 10 at% carbon is written as $FeCrMnNiC_{0.5}$; $FeCrMnNiC_x$ with 6 at% carbon is written as $FeCrMnNiC_{0.3}$; $FeCrMnNiC_x$ with 2 at% carbon is written as $FeCrMnNiC_{0.1}$.

2. Materials and methods

The bulk alloys were synthesised in Vacuum Arc Melting Furnace from powders of iron (Fe), chromium (Cr), manganese (Mn), nickel (Ni) and carbon (C) with a purity at ~ 99.5 (at. %), (99.5, 99.2, 99.9, 99.6 and 99.3) respectively. The compositions were prepared in a volume of around 1 cc with an ingot weight of approximately 8 g. The system with loaded powders was kept for few hours under vacuum ($6x10^{-2}$ Torr) to ensure the powders outgassing. The melts were conducted in the presence of a pure argon flow with a pressure during the melting at around 500 Torr. The melts were repeated five times to make the samples more homogeneous. After the melting the ingots were kept in the furnace under vacuum for around an hour to prevent oxidation. The sample surface then was polished using 120, 240, 600 and 1200 silicon carbide (SiC) sandpaper. The final polishing was done by 1 mic monocrystalline Gemini Diamond Slurry. After that, the samples were cleaned by acetone.

The surface morphology was analysed by FEI Quanta FEG250 Scanning Electron Microscope (SEM) using both secondary electrons (SE) and back scattered electron detectors (BSED). Energy-Dispersive X-ray spectroscopy (EDX), Oxford Instruments, was used to analysis the chemical composition of the samples. It is reasonable in our case to believe that the uncertainty in quantification is at around 2 at%. X-ray diffraction (XRD) was measured by Bruker D2 Phaser instrument under Center 4.0 software.

Potentiodynamic polarization tests were conducted in three-electrode cell arrangements. A saturated calomel electrode (SCE) was used as a reference electrode, platinum as the counter electrode and samples as working electrodes (exposed area of 0.5 cm^2) were used. The corrosion media was aqueous 3.5% NaCl solution. The measurements were done under ambient pressure and at room temperature. The open circuit potential (OCP) was measured for thirty minutes before each test. The potential and current were measured using Autolab potentiostat controlled by Nova 1.10 software. The polarisation curves were used to evaluate the corrosion parameters such as, corrosion current density (i_{corr}), corrosion potential (E_{corr}).

Ion irradiations of $FeCrMnNiC_2$ were performed with 600 keV Xe^{2+} at 623 K using MIAMI-2 (Microscopes and Ion Accelerators for Materials Investigations), in-situ TEM with ion irradiation facility located at the University of Huddersfield [58]. The displacement per atom (dpa) was calculated using SRIM 2013 assuming a sample thickness of about 140 nm with an average atomic density of 8.55×10^{22} atoms/cm^3 for and displacement energies set as 40 eV for all elements [59]. The maximum fluences were 6×10^{15} ions/cm^2, which corresponds to 50 dpa. Gatan Model636 heating holder was used for high temperature irradiation. The irradiated $FeCrMnNiC_{0.02}$ was characterised using bright-field TEM (BF-TEM), selected-area diffraction pattern (SAED) and dark field TEM (DF-TEM).

A Micro Materials Nano Test platform was used to assess the mechanical properties (hardness and modulus). The instrument and the Berkovich nano indenter were calibrated using silica and tungsten samples.

3. Results and discussion

3.1 Microstructure

3.1.1 FeCrMnNiC alloy

An attempt to smelter in low vacuum a high entropy material by the composition was successful. The average chemical composition (Fig. 1a) is close to equiatomic material. The material evidently has element segregation as revealed by BSE (Fig1(b)). Light element enriched phase (e.g., less backscatter electrons – darker shade in the image) has significant chromium and carbide enrichment at the expense of missing other metals. The chemical composition in Fig.1(c) shows equal ratios of Cr and C with significant amount of Fe and Mn.

(a)

Element	Weight%	Atomic%
C K	5.7	21.8
Cr K	22.08	19.51
Mn K	24.2	20.23
Fe K	22.02	18.11
Ni K	26	20.35
Totals	100	

(b)

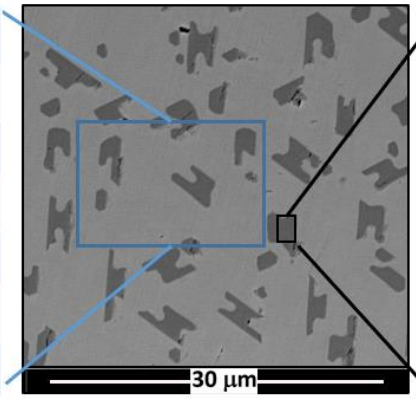

(c)

Element	Weight%	Atomic%
C K	12.55	38.95
Cr K	53.21	38.13
Mn K	14.37	9.74
Fe K	17.36	11.58
Ni K	2.51	1.59
Totals	100.00	

Figure 1. Analysis of microstructure and compositions of equiatomic alloy. (a) – average chemical composition of equiatomic FeCrMnNiC; (b) – BSED surface microstructure image; (c) - chemical composition of the lighter element phase.

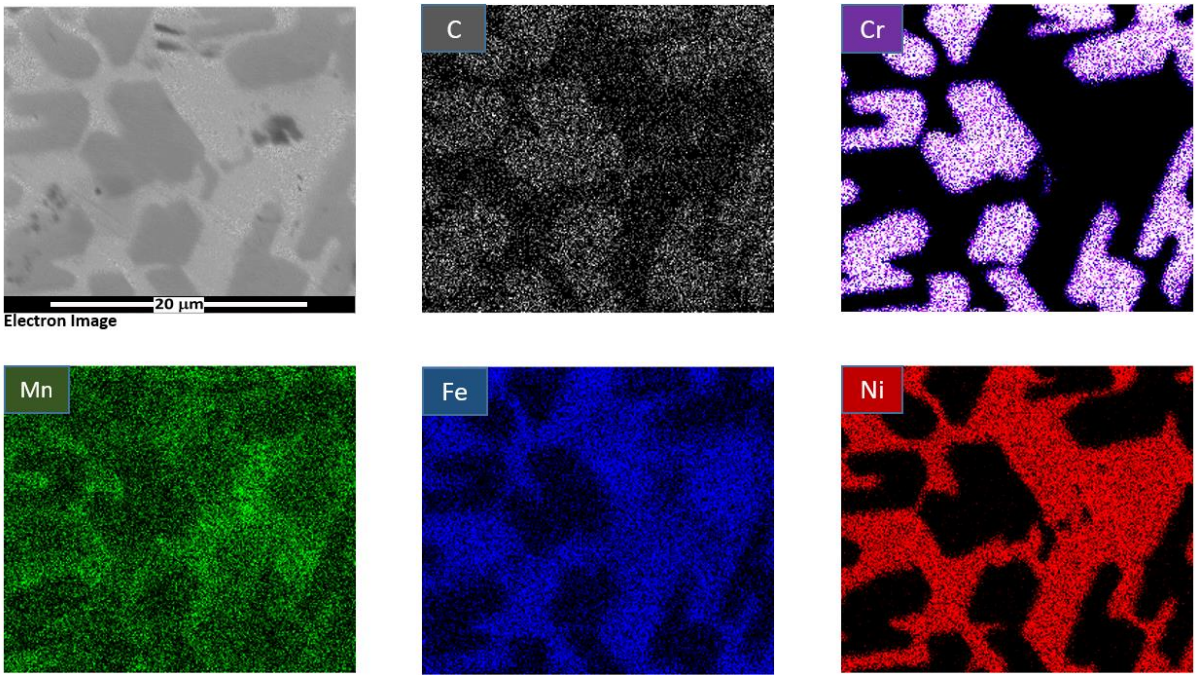

Figure 2. EDX element mapping of FeCrMnNiC bulk alloy.

Figure 2 shows EDX elemental mapping of equiatomic FeCrMnNiC bulk alloy. The mapping clearly demonstrates that the alloy is split into two phases with predominant concentrations of chromium/iron/manganese carbide and Ni/Mn.

It is well known fact that Cr and Fe are strong carbide formers. Usually, the carbides in alloys form compound in line with M_3C, but in FeCrMnNiC carbon rich precipitates are closer to M_2C composition.

3.1.2 $FeCrMnNiC_{0.5}$ alloy

Fig.3(a) demonstrates an average chemical composition of $FeCrMnNiC_{0.5}$ which was analysed by EDX. The material structure (Fig3(b)) again shows segregation of chromium and carbon but the quantification ((Fig3(c)) reveals rather smaller iron segregation into the predominantly carbidic grains.

(a)

Element	Weight%	Atomic%
C K	2.75	11.77
Cr K	22.3	22.04
Mn K	23.3	21.8
Fe K	22.25	20.48
Ni K	27.3	23.91
Totals	100	

(b)

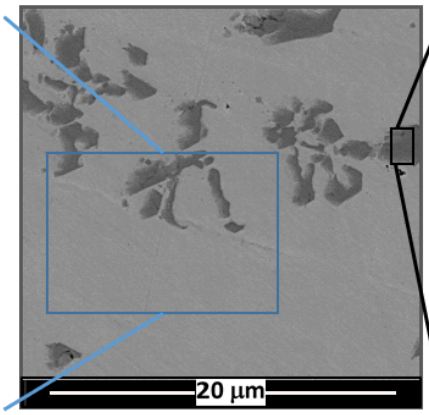

(c)

Element	Weight%	Atomic%
C K	11.84	37.41
Cr K	54.27	39.61
Mn K	15.27	10.55
Fe K	11.75	7.98
Ni K	6.88	4.45
Totals	100.00	

Figure 3. Analysis of microstructure and compositions of $FeCrMnNiC_{0.5}$ alloy. (a) – average chemical composition; (b) – BSED surface microstructure image; (c) - chemical composition of the lighter element phase.

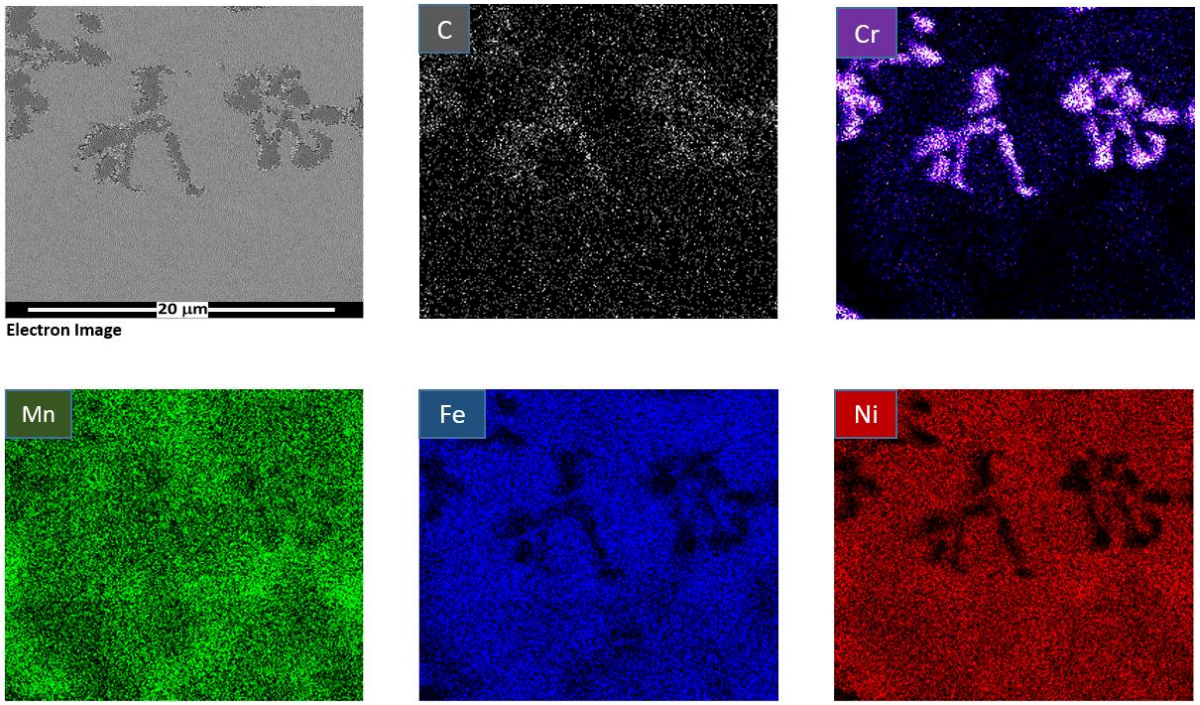

Figure 4. EDX element mapping of FeCrMnNiC with 10 at. % of C bulk alloy.

Fig.4 clearly shows the existence of two compositionally distinctive phases. The maps of carbon and chromium show co-segregation of those elements which is attributed to formation

of predominantly chromium carbides. It is possible to note that Mn is more evenly distributed in this case as compared with the equimolar alloy.

3.1.3 $FeCrMnNiC_{0.3}$ alloy

In the case of $FeCrMnNiC_{0.3}$ the EDX quantifications of distinctive areas (Figs 5(a) and 5(c)) show similar segregation to the higher carbon content alloys. Fig.5(a) shows the atomic percentage (at %) of the alloy is near equiatomic in metals with 6 at % of carbon. The alloy again has at least two phases as it is demonstrated by BSED detector surface microstructure image in Fig.5(b).

(a)

Element	Weight%	Atomic%
C K	1.4	6.15
Cr K	22.36	22.69
Mn K	23.32	22.4
Fe K	25.6	24.21
Ni K	27.3	24.55
Totals	100	

(b)

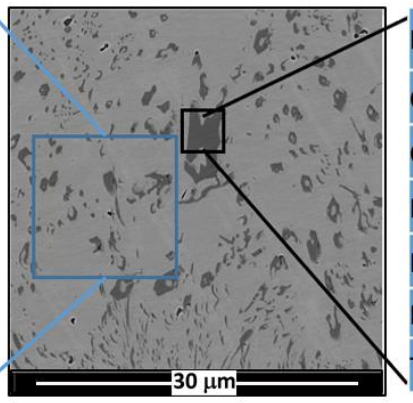

(c)

Element	Weight%	Atomic%
C K	9.19	31.11
Cr K	54.08	42.27
Mn K	15.65	11.58
Fe K	12.73	9.26
Ni K	8.35	5.78
Totals	100.00	

Figure 5. Microstructure analysis in $FeCrMnNiC_x$ alloy with 6 at. % of C: (a) - chemical composition of the alloy; (b) - BSED surface microstructure image at high magnification; (c) - chemical composition of dark area as marked in (b).

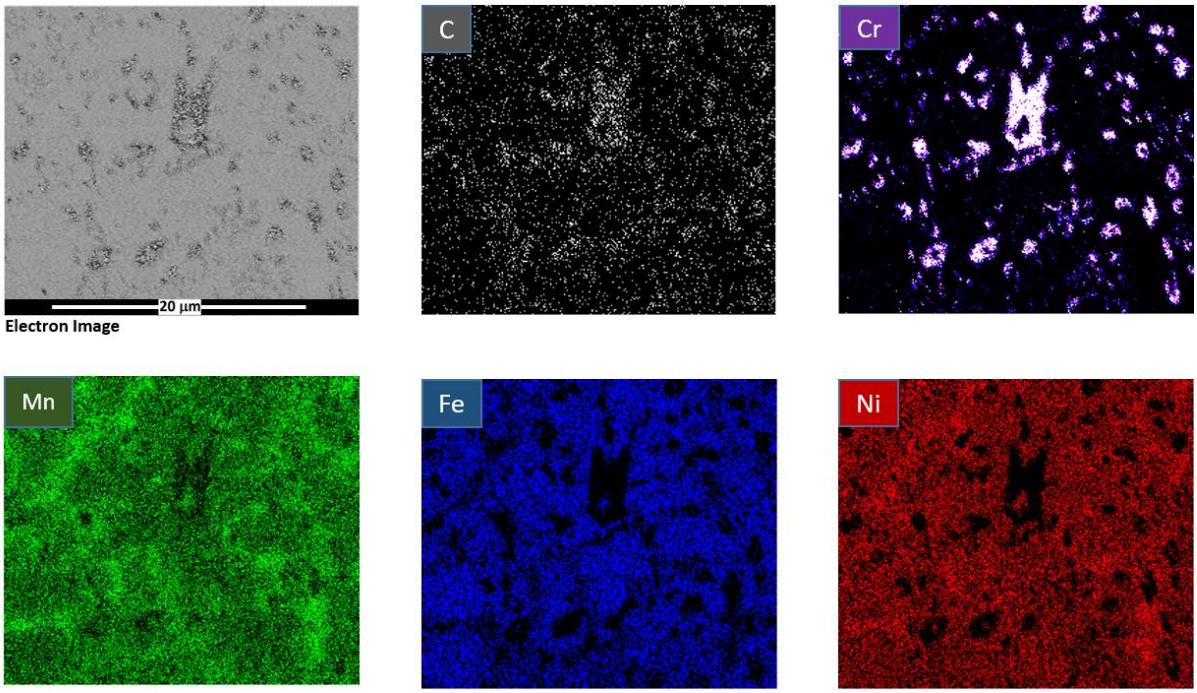

Figure 6. EDX element mapping of $FeCrMnNiC_{0.3}$ bulk alloy.

At the first glance (Fig.5(b)) there one can see only two phases. However, the element mapping also reveals Mn preferential segregation in areas with less Cr/Fe carbides. Moreover, some carbidic phases appear to be plate-like.

3.1.4 $FeCrMnNiC_{0.1}$ alloy

After reducing carbon content to 2 at%, a single-phase alloy with uniform microstructure have been produced as it is provided in BSED SEM surface image shown in figure 7 (a).

(a)

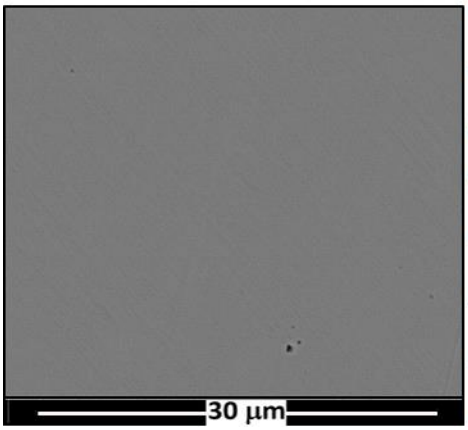

(b)

Element	Weight%	Atomic%
C K	0.53	2.42
Cr K	22.36	23.57
Mn K	23.32	23.27
Fe K	25.64	25.17
Ni K	27.38	25.57
Totals	100.00	

Figure 7. Analysis of surface microstructure of FeCrMnNiC alloy with 2 at. % of C: (a) - BSED surface image; (b) - chemical composition.

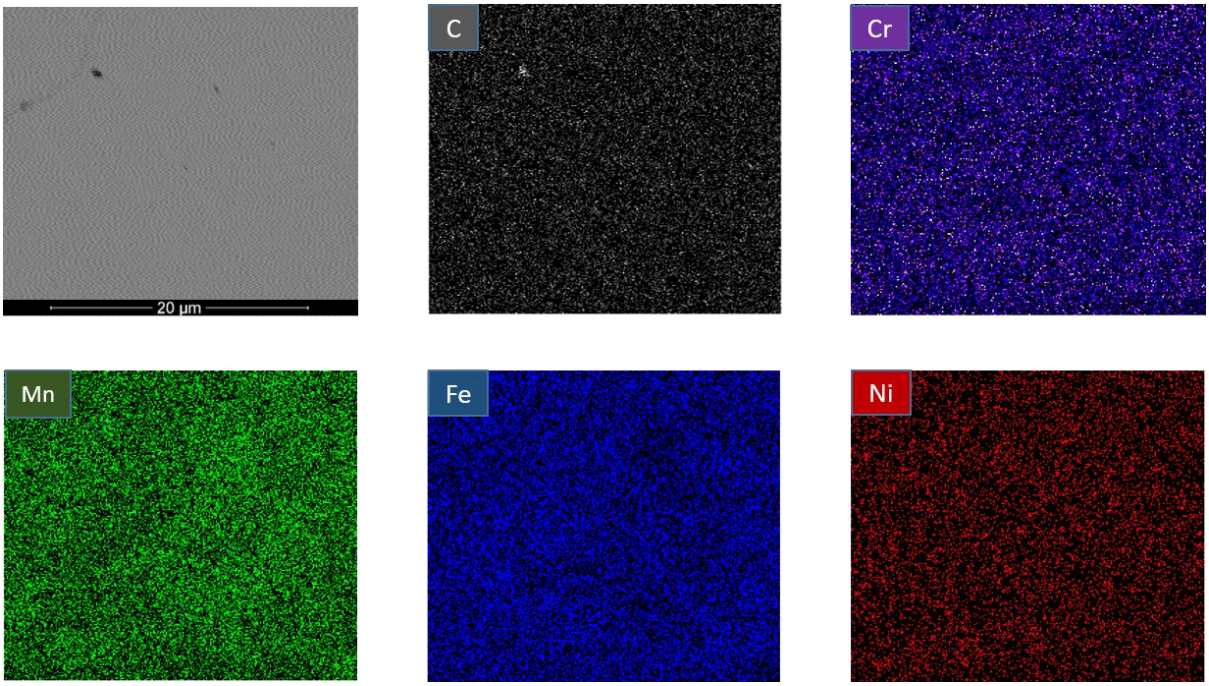

Figure 8. Alloy element EDX mapping in $CrMnNiC_{0.1}$.

The EDX mapping (Fig. 8) confirms that C, Cr, Mn, Fe and Ni are distributed in the material homogeneously without any element separation or precipitation.

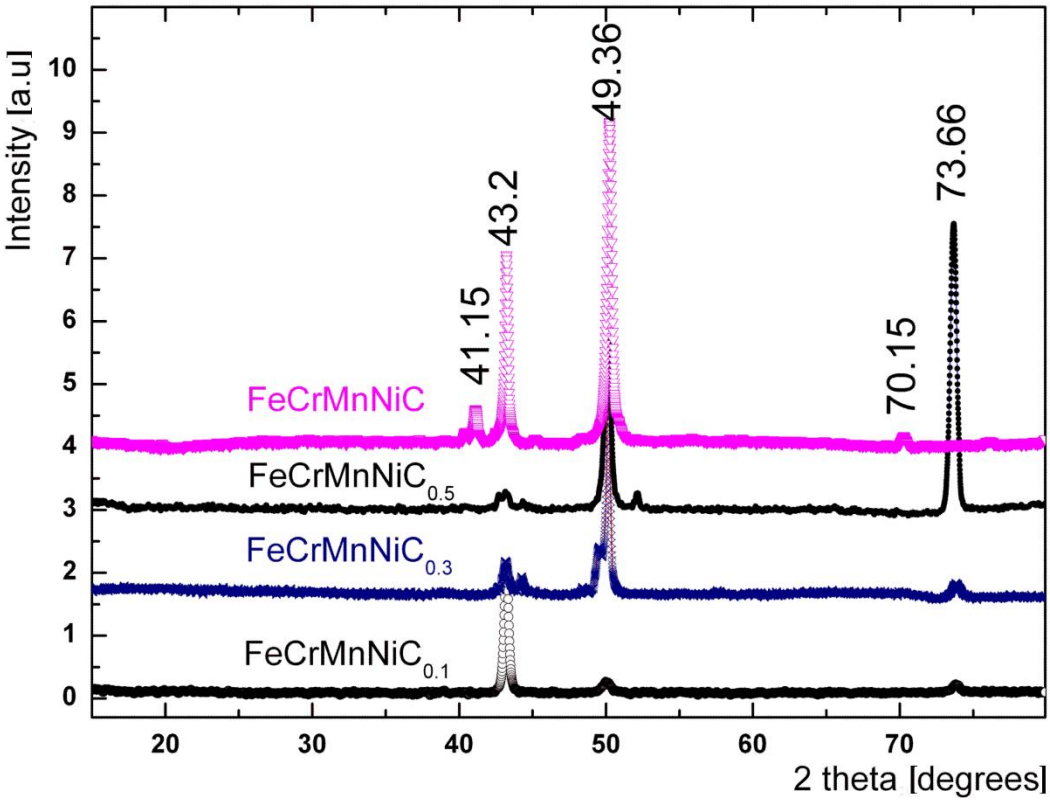

Figure 9. XRD patterns of $FeCrMnNiC_x$ bulk alloys with various carbon content.

XRD patterns of all $FeCrMnNiC_x$ with varying of carbon content are displayed on Fig. 9. It is possible to make a general statement that the patterns are quite complex and cannot be easily deconvoluted into simple BCC or FCC structures as for each composition additional peaks are present and those peaks cannot be simply indexed. It is probably easier to start with $CrMnNiC_{0.1}$ as the material does not have visible element segregation. In this case the main peak at 43.2^0 can be attributed to (111) peak in FCC phase in line previously published work on NiCoFeCr with Al [60] and similar alloy with Co [61]. The peaks (200) and (220) at 49.93^0 and 73.66^0 correspondingly belong also to the FCC phase.

Increase of carbon content to 6 at% immediately complicates the diffraction peak structure as additional phases appear (we know this also from the SEM analysis). The peaks at 44.15^0 and 49.36^0 might belong to so named BCC and BCC/B2 phases [62].

The material at 10 at % C develops a phase which has very strong reflection at 73.66^0 (possibly (220) peak for FCC structure). This peak intensity rise looks like a texturing due the alloy deformation (see for instance [61]), but the sample has not been deformed. It is possible to assume that the peak is due to high stresses in the material due to more extensive carbide formation. A low intensity peak at 52.3^0 probably indicates as one of secondary phases CrC [63].

The XRD spectra reflects but another material structure transformation when carbon content increases to 20 at%. The previous (220) peak completely disappears. The two small intensity

peaks at (41.15^0 & 70.15^0) can be secondary phases of chromium carbides [63]. Two high intensity peaks probably belong to the previously observed FCC structure.

While one can argue that carbides in steels should be reasonably well understood, but complex concentrated alloy with carbon during thorough analysis still reveal new complex phases [64]. Formation of single phase high entropy alloys believed to be limited by the possible limited lattice distortion effects, which can be calculated as so named δ parameter [65]. It has been already shown by many researchers that the formation of single phase HEA by arc melting of bulk form only can be achieved when the difference between the atomic sizes is low (the δ value found to be < 8.6). In addition, if the entropy mixing is high, it enhances the formation of single phase [65].

We, on our part and at this time, will cease the XRD analysis as our main focus was on a single-phase material and its properties.

3.2 Corrosion test

Potentiodynamic polarisation curve results for FeCrMnNiC bulk alloys are revealed in Fig. 10. The numerical corrosion parameters (i_{corr} & E_{corr}) of FeCrMnNiC bulk alloys are provided in Table 1. The results confirm that as the amount of carbon increases, the resistance to corrosion increases for high content carbon content FeCrMnNiC alloys.

Table 1. Corrosion parameters of $FeCrMnNiC_x$ bulk alloys.

Alloy	i_{corr}, A/cm^2	E_{corr}, *v*
$FeCrMnNiC_{0.1}$	7.3*E-7	-0.36
$FeCrMnNiC_{0.3}$	2.2*E-7	-0.34
$FeCrMnNiC_{0.5}$	2.3*E-7	-0.32
FeCrMnNiC	1.5*E-7	-0.28

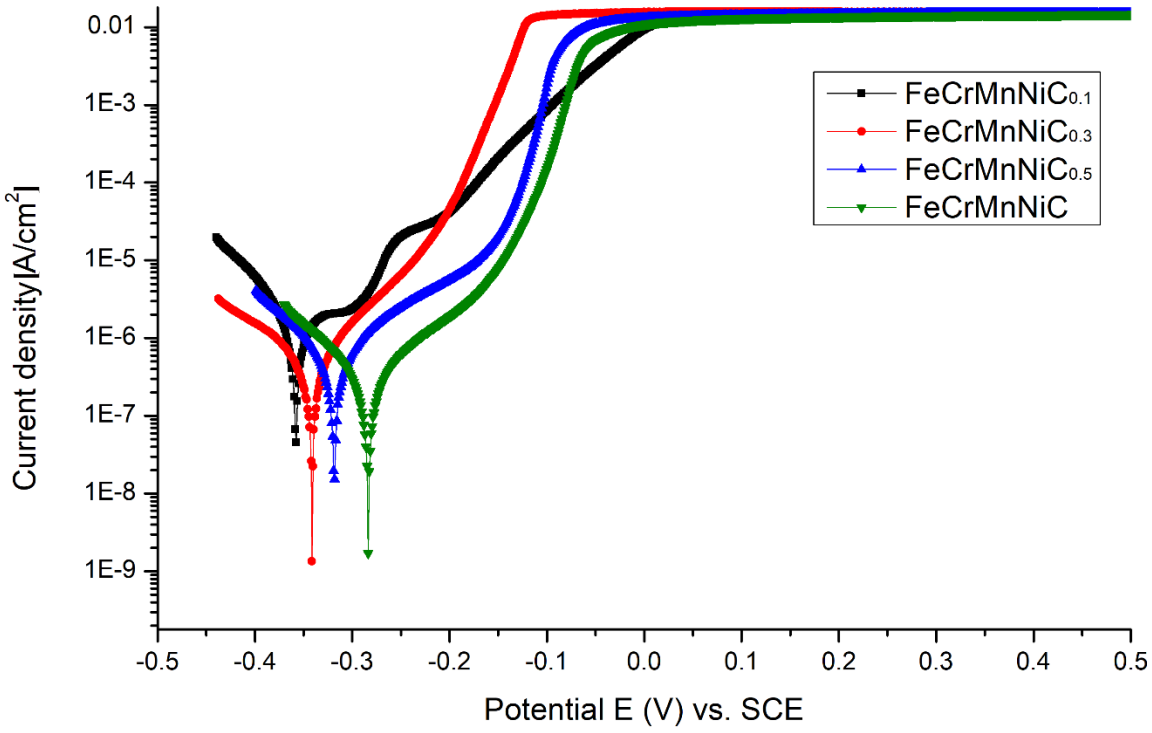

Figure 10. Potentiodynamic polarisation curves of $FeCrMnNiC_x$ bulk alloys.

According to electrochemical practise, a material has good resistance to corrosion when the corrosion potential E_{corr} increases to becomes more positive and this is accompanied by a reduction of corrosion current density i_{corr} [66, 67]. All our alloys exhibited similar corrosion behaviour but with different corrosion parameters. It can be noticed from the polarisation curve on Fig. 10 that the corrosion potential moves towards higher cathodic as carbon concentration increases from 2 to 20 at. % in $FeCrMnNiC_x$ alloys. The corrosion potential ($E_{corr,}$) had improved from -0.36 to -0.28 V. The corrosion current density (i_{corr}, A/cm^2) decreased from 7.3E^{-7} to 1.5E^{-7} as carbon content increase. Apart from the influence of carbon and carbides it is possible to assume that higher corrosion resistance is mediated by high entropy effect [10]. In other words, the cocktail effect of traditional elements (Cr and Ni), which have high corrosion resistance by themselves, improves the resistance to corrosion of the alloy [68]. Adding a metalloid like carbon to the alloy, further improves the resistance to corrosion [69]. Formation of CrC_x (chromium carbide) phase with a small content of manganese believed to have good corrosion resistance too [70]. The above results are in a way similar to other colleague earlier results, where the effect of Molybdenum (Mo) found to be beneficial and enhances the corrosion resistance of $CoCrFeNiMo_x$, as CrMo phase played the main role to improve the corrosion resistance [71].

At this point we have to admit that the same equiatomic composition FeCrMnNiC but as an amorphous coating, where mixing entropy probably was realised more fully, had exhibited much better corrosion performance (E_{corr}=0.07V, i_{corr}=2.5E-10 A/cm^2) [57].

3.3 Irradiation test of $FeCrMnNiC_{0.1}$

Material requirements for nuclear energy generation are most stringent – any deviation from the material initial properties is viewed as damage. It is possible to say that materials with less complex initial structure might be of more interest as they are expected to be less inclined to damage accumulation. From this point of view, it is more prudent to study the irradiation of $FeCrMnNiC_{0.1}$ alloy. 350 keV Xe^{+} ion damage represents the harshest radiation environment as it produces more than 2000 atom displacements for each impeding ion. The calculated damage (e.g. atom displacement profile) as calculated by SRIM 2013 with displacement energy set to 40 eV for all atoms [59] is presented at Fig.11.

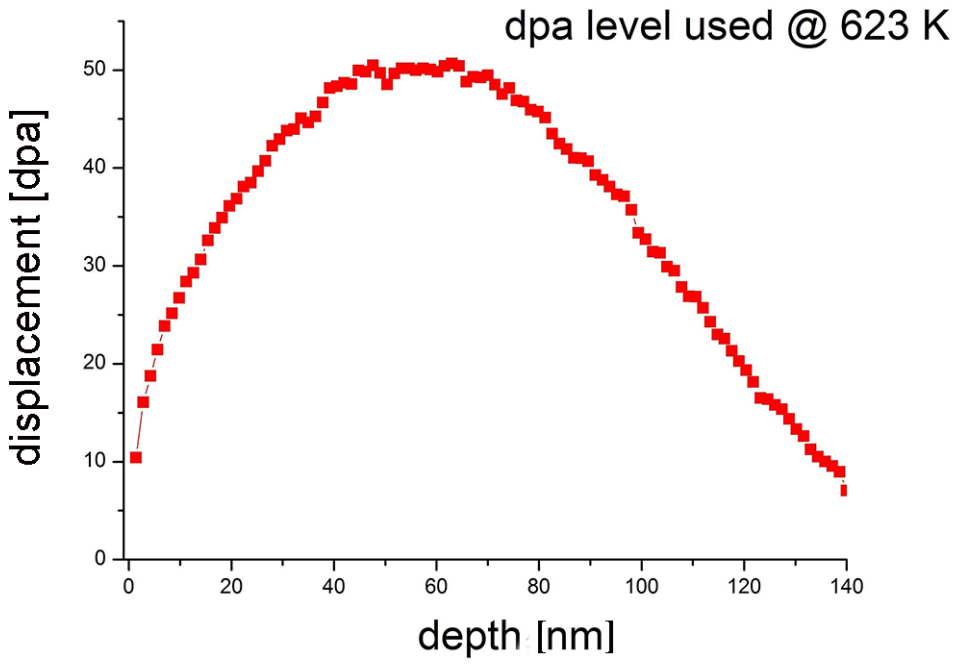

Figure 11. Atom displacement profile as produced by SRIM-2013, peak fluence of 6 x 10^{15} ions.cm^{-2} and sample thickness of 140 nm. Displacement energy for all elements 40 eV.

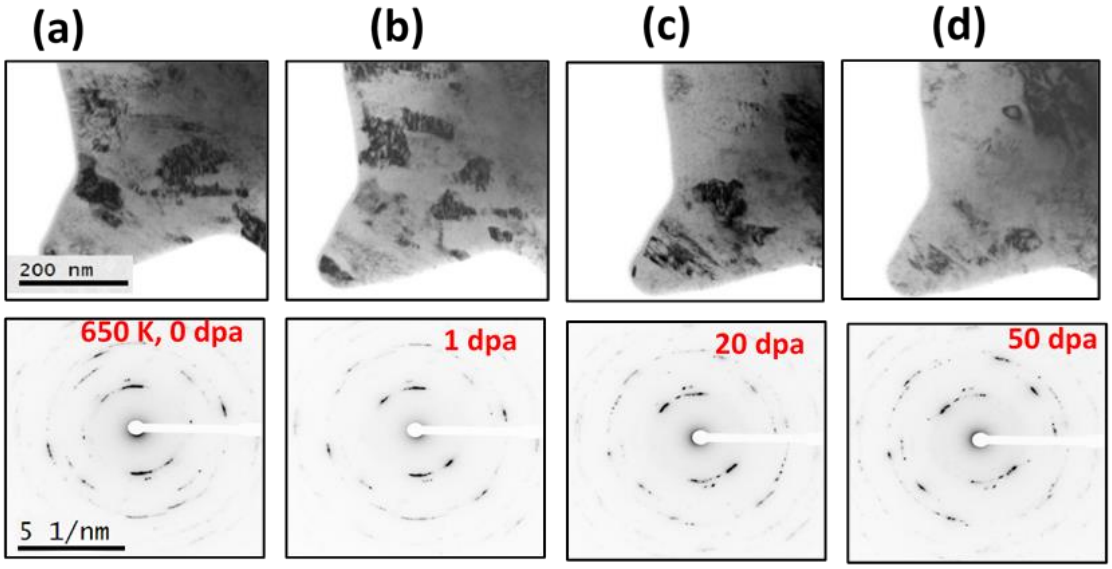

Figure 12. BFTEM and SAED images of nanocrystalline $FeCrMnNiC_{0.1}$ alloy: (a)-(d) – data for as sintered and in-situ ion irradiated alloy at 623 K.

It is possible to see (Fig. 12) that as-sintered $FeCrMnNiC_{0.1}$ alloy has nanocrystalline structure. The crystal sizes are varying from 30 -110 nm and the alloy SAED demonstrates nanocrystal diffraction possibly with some texturing. Both, BFTEM images and SAED patterns do not display any observable damage even after irradiation to 50 dpa. The only observable effects are some reorientation of nano crystals and same additional crystal diffraction structure as seen in SAED.

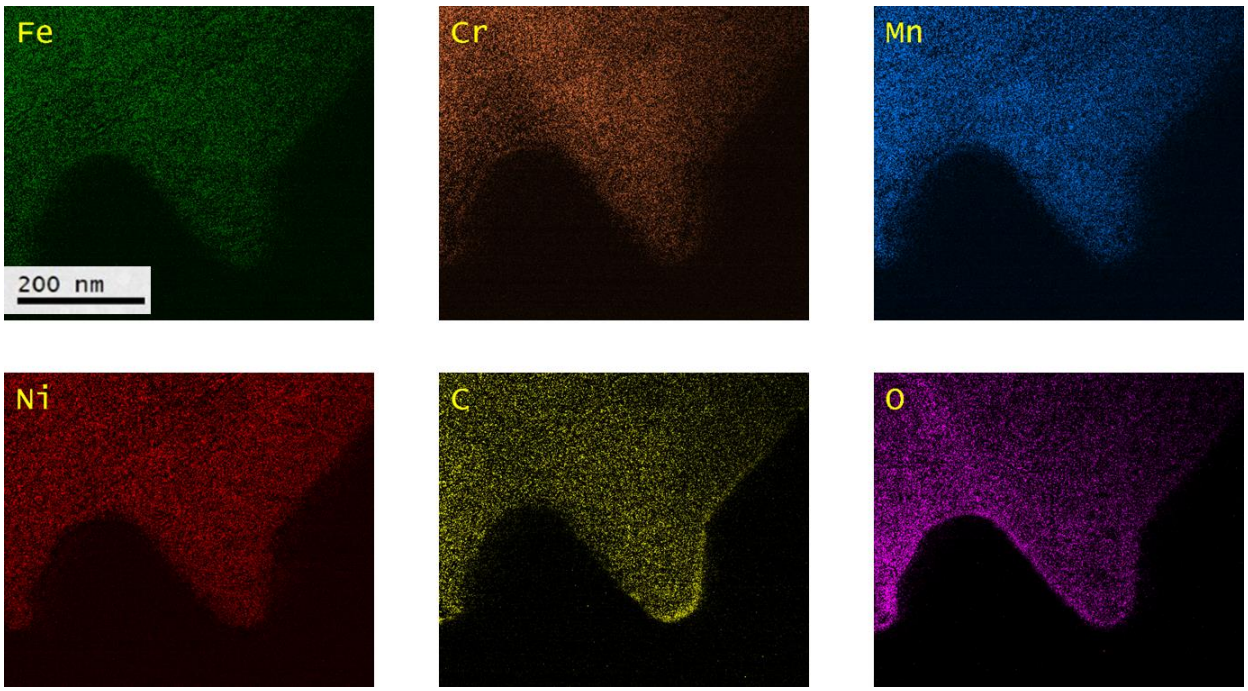

Figure 13. EFTEM images of irradiated to 50 dpa $FeCrMnNiC_{0.1}$ alloy.

Energy filtered TEM (EFTEM) imaging of the alloy after irradiation (see Fig.13) demonstrates even distribution for all elements without any element segregation or precipitation. This superior irradiation resistance was believed due to severe lattice distortion and sluggish diffusion that are unique to HEAs [44]. In addition, the resistance to defect formation during irradiation was attributed to the presence of nanocrystalline forming high density of grain boundaries [72].

4. Mechanical properties

The hardness measurements were done for the single-phase $FeCrMnNiC_{0.1}$ alloy. The indentation load was gradually increased from 20 to 50 mN. The results showed that the alloy has a hardness of 7.5 ± 0.84GPa. Reduced Young's modulus was at 250±28.1 GPa when approximated to zero load indentation.

The high hardness of the single-phase alloy $FeCrMnNiC_{0.1}$ can be attributed to the effect of solid solution hardening effect [73]. It is also plausible to assume that the hardness is partially provided by the compositional homogeneity and partial alloying formation which lead to strengthening of bonding structure [74]. The results demonstrate that the addition of carbon in small concentration to high entropy alloy can be beneficial to increase the alloy hardness. This is in agreement with findings of other groups when adding carbon to CoCrFeNiC [51] and $FeCoCrNiW_{0.3}$+5 at% of C [52] had led to better mechanical properties.

5. Conclusion

$FeCrMnNiC_x$ (x= 2,5,10 and 20 at. %) alloys were produced by vacuum arc melting in search for a single-phase bulk alloy in the $FeCrMnNiC_x$ system. Only $FeCrMnNiC_x$ at x= 2 at. % was found to be a single-phase alloy as confirmed by BSE imaging, EDX mapping and TEM. At the higher carbon content in the $FeCrMnNiC_x$ (x= 5, 10 and 20 at. %) at least two phases are observed. In fact, the number of phases could be even higher, but it was regarded as being outside of the main interest at the moment. All synthesised alloys were electrochemically tested in 3.5 wt. % NaCl solution to evaluate the corrosion resistance. The alloys get nobler and more corrosion resistant as the amount of carbon content grows. However, comparison the corrosion properties with the amorphous thin film FeCrMnNiC demonstrates that not fully randomised lattice positions and possibly grain boundaries weaken the corrosion resistance. Heavy ion irradiations of $FeCrMnNiC_{0.1}$ performed with 600 KeV Xe^{2+} to a maximum displacement level of 50 dpa at 623 K indicated radiation resistance to phase transformation and element separation. It is possible to assume that good mechanical properties of $FeCrMnNiC_{0.1}$ alloy and demonstrated radiation resistance can make the material a candidate for applications in extreme environments. The $FeCrMnNiC_{0.1}$ alloy showed a hardness of 7.5 ± 0.84GPa, and reduced Young's modulus of 250 ± 28.1 GPa.

Data availability

No additional data are available.

CRediT authorship contribution statement

Waleed Muftah: conceptualization, investigation, methodology, data curation, formal analysis, writing - original draft, preparation. Vladimir Vishnyakov: supervision, writing - review & editing.

Declaration of interests

The authors declare that they have no known competing financial interests or personal relationships that could have appeared to influence the work reported in this paper.

Acknowledgement

The authors appreciatively acknowledge the use of facilities in the MIAMI (Microscope and Ion Accelerator for Materials Investigation. And special appreciations to Mr Mohammed Imtyazuddin a PhD in Nuclear Materials who prepared sample by FIB & conducted *in-situ* TEM irradiation examination. Author appreciations also go to Dr Anamul Haq Jeri Mir EPSRC Early Career Research Fellow who assisted with *in-situ* irradiation.

References:

[1] J.W. Yeh, S.K. Chen, S.J. Lin, J.Y. Gan, T.S. Chin, T.T. Shun, C.H. Tsau, S.Y. Chang, Nanostructured high-entropy alloys with multiple principal elements: novel alloy design concepts and outcomes, Advanced Engineering Materials 6(5) (2004) 299-303.
[2] J.-W. Yeh, S.-J. Lin, T.-S. Chin, J.-Y. Gan, S.-K. Chen, T.-T. Shun, C.-H. Tsau, S.-Y. Chou, Formation of simple crystal structures in Cu-Co-Ni-Cr-Al-Fe-Ti-V alloys with multiprincipal metallic elements, Metallurgical and Materials Transactions A 35(8) (2004) 2533-2536.
[3] D. Wang, Y. Li, B. Sun, M. Sui, K. Lu, E. Ma, Bulk metallic glass formation in the binary Cu–Zr system, Applied Physics Letters 84(20) (2004) 4029-4031.
[4] D. Xu, B. Lohwongwatana, G. Duan, W.L. Johnson, C. Garland, Bulk metallic glass formation in binary Cu-rich alloy series–Cu100− xZrx (x= 34, 36, 38.2, 40 at.%) and mechanical properties of bulk Cu64Zr36 glass, Acta Materialia 52(9) (2004) 2621-2624.
[5] L. Xia, W. Li, S. Fang, B. Wei, Y. Dong, Binary Ni–Nb bulk metallic glasses, AIP, 2006.
[6] F. Zhang, M. Zhang, B. Lv, J. Li, Effect of high-energy-density pulse current on solidification microstructure of FeCrNi alloy, Mater. Sci 13(2) (2007) 120-122.
[7] D.B. Miracle, O.N. Senkov, A critical review of high entropy alloys and related concepts, Acta Materialia 122 (2017) 448-511.
[8] J. Jensen, B. Welk, R. Williams, J. Sosa, D. Huber, O. Senkov, G. Viswanathan, H. Fraser, Characterization of the microstructure of the compositionally complex alloy Al1Mo0. 5Nb1Ta0. 5Ti1Zr1, Scripta Materialia 121 (2016) 1-4.
[9] J. Rodríguez, F. De Zan, P.S. Agram, J.G. Álvarez, S. Mukherjee, D. Tedesco, A. Tava, F. Pellati, L. Mercolini, R. Sardella, Keyword, Remote Sensing 3 (2019).
[10] Y. Qiu, Y. Hu, A. Taylor, M. Styles, R. Marceau, A. Ceguerra, M. Gibson, Z. Liu, H. Fraser, N. Birbilis, A lightweight single-phase AlTiVCr compositionally complex alloy, Acta Materialia 123 (2017) 115-124.
[11] S. Gorsse, J.-P. Couzinié, D.B. Miracle, From high-entropy alloys to complex concentrated alloys, Comptes Rendus Physique 19(8) (2018) 721-736.
[12] S. Gorsse, D.B. Miracle, O.N. Senkov, Mapping the world of complex concentrated alloys, Acta Materialia 135 (2017) 177-187.
[13] S. Gorsse, M. Nguyen, O.N. Senkov, D.B. Miracle, Database on the mechanical properties of high entropy alloys and complex concentrated alloys, Data in brief 21 (2018) 2664-2678.
[14] Z. Wu, H. Bei, G.M. Pharr, E.P. George, Temperature dependence of the mechanical properties of equiatomic solid solution alloys with face-centered cubic crystal structures, Acta Materialia 81 (2014) 428-441.
[15] T. Zuo, R. Li, X. Ren, Y. Zhang, Effects of Al and Si addition on the structure and properties of CoFeNi equal atomic ratio alloy, Journal of Magnetism and Magnetic Materials 371 (2014) 60-68.
[16] Z. Leong, Y. Huang, M. Bloomfield, B. Jim, G. Kerridge, J. Pitcairn, M. Schobitz, L. Sinclair, S. Zilinskaite, R. Goodall, Refining As-Cast Structures of Novel SixTiVCrZr High-Entropy Alloys Using Estimated Effective Solidification Temperature Obtained Using Chvorinov's Rule, Metals 10(3) (2020) 317.
[17] Y. Gan, W. Wang, Z. Guan, Z. Cui, Multi-layer laser solid forming of Zr65Al7. 5Ni10Cu17. 5 amorphous coating: Microstructure and corrosion resistance, Optics & Laser Technology 69 (2015) 17-22.
[18] G.R. Holcomb, J. Tylczak, C. Carney, Oxidation of CoCrFeMnNi High Entropy Alloys, JOM 67(10) (2015) 2326-2339.
[19] C. Lee, Y. Chen, C. Hsu, J. Yeh, H. Shih, Enhancing pitting corrosion resistance of AlxCrFe1. 5MnNi0. 5 high-entropy alloys by anodic treatment in sulfuric acid, Thin Solid Films 517(3) (2008) 1301-1305.
[20] D. Miracle, Critical assessment 14: High entropy alloys and their development as structural materials, Materials Science and Technology 31(10) (2015) 1142-1147.
[21] D. Xiao, P. Zhou, W. Wu, H. Diao, M. Gao, M. Song, P. Liaw, Microstructure, mechanical and corrosion behaviors of AlCoCuFeNi-(Cr, Ti) high entropy alloys, Materials & Design 116 (2017) 438-447.
[22] T. Zhang, L. Xin, F. Wu, R. Zhao, J. Xiang, M. Chen, S. Jiang, Y. Huang, S. Chen, Microstructure and mechanical properties of FexCoCrNiMn high-entropy alloys, Journal of Materials Science & Technology 35(10) (2019) 2331-2335.

[23] S.J. Mary, N. Rajan, R. Epshiba, High entropy alloys properties and its applications–An over view, European Chemical Bulletin 4(4-6) (2015) 279-284.
[24] B. Murty, J. Yeh, S. Ranganathan, High-entropy alloys. 2014, Butterworth-Heinemann.
[25] M.A. Hemphill, T. Yuan, G. Wang, J. Yeh, C. Tsai, A. Chuang, P. Liaw, Fatigue behavior of Al0. 5CoCrCuFeNi high entropy alloys, Acta Materialia 60(16) (2012) 5723-5734.
[26] H.B. Cui, L.F. Zheng, J.Y. Wang, Microstructure evolution and corrosion behavior of directionally solidified FeCoNiCrCu high entropy alloy, Applied Mechanics and Materials, Trans Tech Publ, 2011, pp. 146-149.
[27] Z. Li, K.G. Pradeep, Y. Deng, D. Raabe, C.C. Tasan, Metastable high-entropy dual-phase alloys overcome the strength–ductility trade-off, Nature 534(7606) (2016) 227-230.
[28] B. Gludovatz, A. Hohenwarter, D. Catoor, E.H. Chang, E.P. George, R.O. Ritchie, A fracture-resistant high-entropy alloy for cryogenic applications, Science 345(6201) (2014) 1153-1158.
[29] C.-Y. Hsu, C.-C. Juan, T.-S. Sheu, S.-K. Chen, J.-W. Yeh, Effect of aluminum content on microstructure and mechanical properties of Al x CoCrFeMo 0.5 Ni high-entropy alloys, Jom 65(12) (2013) 1840-1847.
[30] Z. Li, S. Zhao, R.O. Ritchie, M.A. Meyers, Mechanical properties of high-entropy alloys with emphasis on face-centered cubic alloys, Progress in Materials Science 102 (2019) 296-345.
[31] P. Sarker, T. Harrington, C. Toher, C. Oses, M. Samiee, J.-P. Maria, D.W. Brenner, K.S. Vecchio, S. Curtarolo, High-entropy high-hardness metal carbides discovered by entropy descriptors, Nature communications 9(1) (2018) 1-10.
[32] M.-H. Tsai, C.-W. Wang, C.-W. Tsai, W.-J. Shen, J.-W. Yeh, J.-Y. Gan, W.-W. Wu, Thermal stability and performance of NbSiTaTiZr high-entropy alloy barrier for copper metallization, Journal of the Electrochemical Society 158(11) (2011) H1161-H1165.
[33] B. Gorr, M. Azim, H.-J. Christ, T. Mueller, D. Schliephake, M. Heilmaier, Phase equilibria, microstructure, and high temperature oxidation resistance of novel refractory high-entropy alloys, Journal of Alloys and Compounds 624 (2015) 270-278.
[34] M.-H. Chuang, M.-H. Tsai, W.-R. Wang, S.-J. Lin, J.-W. Yeh, Microstructure and wear behavior of AlxCo1. 5CrFeNi1. 5Tiy high-entropy alloys, Acta Materialia 59(16) (2011) 6308-6317.
[35] Y. Qiu, M. Gibson, H. Fraser, N. Birbilis, Corrosion characteristics of high entropy alloys, Materials Science and Technology 31(10) (2015) 1235-1243.
[36] S. Nene, M. Frank, K. Liu, S. Sinha, R. Mishra, B. McWilliams, K. Cho, Corrosion-resistant high entropy alloy with high strength and ductility, Scripta Materialia 166 (2019) 168-172.
[37] Q. Zhou, S. Sheikh, P. Ou, D. Chen, Q. Hu, S. Guo, Corrosion behavior of Hf0. 5Nb0. 5Ta0. 5Ti1. 5Zr refractory high-entropy in aqueous chloride solutions, Electrochemistry Communications 98 (2019) 63-68.
[38] Y. Shi, B. Yang, X. Xie, J. Brechtl, K.A. Dahmen, P.K. Liaw, Corrosion of Al xCoCrFeNi high-entropy alloys: Al-content and potential scan-rate dependent pitting behavior, Corrosion Science 119 (2017) 33-45.
[39] C. Lee, C. Chang, Y. Chen, J. Yeh, H. Shih, Effect of the aluminium content of AlxCrFe1. 5MnNi0. 5 high-entropy alloys on the corrosion behaviour in aqueous environments, Corrosion Science 50(7) (2008) 2053-2060.
[40] Y. Chou, J. Yeh, H. Shih, The effect of molybdenum on the corrosion behaviour of the high-entropy alloys Co1. 5CrFeNi1. 5Ti0. 5Mox in aqueous environments, Corrosion Science 52(8) (2010) 2571-2581.
[41] H.-d. Wang, J.-n. Liu, Z.-g. Xing, G.-Z. Ma, X.-f. Cui, G. Jin, B.-s. Xu, Microstructure and corrosion behaviour of AlCoFeNiTiZr high-entropy alloy films, Surface Engineering 36(1) (2020) 78-85.
[42] P. Malinovskis, S. Fritze, L. Riekehr, L. von Fieandt, J. Cedervall, D. Rehnlund, L. Nyholm, E. Lewin, U. Jansson, Synthesis and characterization of multicomponent (CrNbTaTiW) C films for increased hardness and corrosion resistance, Materials & Design 149 (2018) 51-62.
[43] K. Jin, C. Lu, L. Wang, J. Qu, W. Weber, Y. Zhang, H. Bei, Effects of compositional complexity on the ion-irradiation induced swelling and hardening in Ni-containing equiatomic alloys, Scripta Materialia 119 (2016) 65-70.
[44] N.K. Kumar, C. Li, K. Leonard, H. Bei, S. Zinkle, Microstructural stability and mechanical behavior of FeNiMnCr high entropy alloy under ion irradiation, Acta Materialia 113 (2016) 230-244.
[45] C. Lu, L. Niu, N. Chen, K. Jin, T. Yang, P. Xiu, Y. Zhang, F. Gao, H. Bei, S. Shi, Enhancing radiation tolerance by controlling defect mobility and migration pathways in multicomponent single-phase alloys, Nature communications 7(1) (2016) 1-8.

[46] T. Nagase, P.D. Rack, J.H. Noh, T. Egami, In-situ TEM observation of structural changes in nano-crystalline CoCrCuFeNi multicomponent high-entropy alloy (HEA) under fast electron irradiation by high voltage electron microscopy (HVEM), Intermetallics 59 (2015) 32-42.
[47] M.A. Tunes, H. Le, G. Greaves, C.G. Schön, H. Bei, Y. Zhang, P.D. Edmondson, S.E. Donnelly, Investigating sluggish diffusion in a concentrated solid solution alloy using ion irradiation with in situ TEM, Intermetallics 110 (2019) 106461.
[48] M.A. Tunes, V.M. Vishnyakov, S.E. Donnelly, Synthesis and characterisation of high-entropy alloy thin films as candidates for coating nuclear fuel cladding alloys, Thin Solid Films 649 (2018) 115-120.
[49] S. Kang, Y.-S. Jung, J.-H. Jun, Y.-K. Lee, Effects of recrystallization annealing temperature on carbide precipitation, microstructure, and mechanical properties in Fe–18Mn–0.6 C–1.5 Al TWIP steel, Materials Science and Engineering: A 527(3) (2010) 745-751.
[50] H. Zuhailawati, T.C. Geok, P. Basu, Microstructure and hardness characterization of mechanically alloyed Fe–C elemental powder mixture, Materials & Design 31(4) (2010) 2211-2215.
[51] T. Huang, L. Jiang, C. Zhang, H. Jiang, Y. Lu, T. Li, Effect of carbon addition on the microstructure and mechanical properties of CoCrFeNi high entropy alloy, Science China Technological Sciences 61(1) (2018) 117-123.
[52] M.G. Poletti, G. Fiore, F. Gili, D. Mangherini, L. Battezzati, Development of a new high entropy alloy for wear resistance: FeCoCrNiW0. 3 and FeCoCrNiW0. 3+ 5 at.% of C, Materials & Design 115 (2017) 247-254.
[53] H. Cheng, H. Wang, Y. Xie, Q. Tang, P. Dai, Controllable fabrication of a carbide-containing FeCoCrNiMn high-entropy alloy: microstructure and mechanical properties, Materials Science and Technology 33(17) (2017) 2032-2039.
[54] S. Shen, F. Chen, X. Tang, J. Lin, G. Ge, J. Liu, Effects of carbon doping on irradiation resistance of Fe38Mn40Ni11Al4Cr7 high entropy alloys, Journal of Nuclear Materials 540 (2020) 152380.
[55] S. Fritze, F. Hahn, L. Riekehr, B. Osinger, E. Lewin, J.M. Schneider, U. Jansson, Influence of carbon on microstructure and mechanical propertiesof magnetron sputtered TaW coatings, Materials and Design 196 (2020) 109070.
[56] Z. Wu, H. Bei, F. Otto, G.M. Pharr, E.P. George, Recovery, recrystallization, grain growth and phase stability of a family of FCC-structured multi-component equiatomic solid solution alloys, Intermetallics 46 (2014) 131-140.
[57] W. Muftah, N. Patmore, V. Vishnyakov, Demanding applications in harsh environment–FeCrMnNiC amorphous equiatomic alloy thin film, Materials Science and Technology 36(12) (2020) 1301-1307.
[58] G. Greaves, A. Mir, R. Harrison, M. Tunes, S. Donnelly, J. Hinks, New microscope and ion accelerators for materials investigations (MIAMI-2) system at the University of Huddersfield, Nuclear Instruments and Methods in Physics Research Section A: Accelerators, Spectrometers, Detectors and Associated Equipment 931 (2019) 37-43.
[59] R.E. Stoller, M.B. Toloczko, G.S. Was, A.G. Certain, S. Dwaraknath, F.A. Garner, On the use of SRIM for computing radiation damage exposure, Nuclear instruments and methods in physics research section B: beam interactions with materials and atoms 310 (2013) 75-80.
[60] Y. Ma, B. Jiang, C. Li, Q. Wang, C. Dong, P.K. Liaw, F. Xu, L. Sun, The BCC/B2 morphologies in AlxNiCoFeCr high-entropy alloys, Metals 7(2) (2017) 57.
[61] J.W. Bae, J. Moon, M.J. Jang, D.-H. Ahn, S.-H. Joo, J. Jung, D. Yim, H.S. Kim, Deep drawing behavior of CoCrFeMnNi high-entropy alloys, Metallurgical and Materials Transactions A 48(9) (2017) 4111-4120.
[62] W.-R. Wang, W.-L. Wang, J.-W. Yeh, Phases, microstructure and mechanical properties of AlxCoCrFeNi high-entropy alloys at elevated temperatures, Journal of Alloys and Compounds 589 (2014) 143-152.
[63] S.M. Schmuecker, D. Clouser, T.J. Kraus, B.M. Leonard, Synthesis of metastable chromium carbide nanomaterials and their electrocatalytic activity for the hydrogen evolution reaction, Dalton Transactions 46(39) (2017) 13524-13530.
[64] G. Tirumalasetty, C. Fang, J. Jansen, T. Yokosawa, M. Boeije, J. Sietsma, M. Van Huis, H. Zandbergen, Structural tale of two novel (Cr, Mn) C carbides in steel, Acta materialia 78 (2014) 161-172.
[65] S. Guo, C. Ng, Z. Wang, C. Liu, Solid solutioning in equiatomic alloys: limit set by topological instability, Journal of Alloys and Compounds 583 (2014) 410-413.
[66] J.R. Davis, ASM Handbook: Nondestructive evaluation and quality control, ASM International1989.

[67] D. Pletcher, F.C. Walsh, Industrial electrochemistry, Springer Science & Business Media2012.
[68] Y. Tian, C. Lu, Y. Shen, X. Feng, Microstructure and corrosion property of CrMnFeCoNi high entropy alloy coating on Q235 substrate via mechanical alloying method, Surfaces and Interfaces 15 (2019) 135-140.
[69] R.S. Henderson, G.A. Shreve, M.A. Tenhover, Enhanced corrosion resistant amorphous metal alloy coatings, Google Patents, 1989.
[70] K. Nygren, M. Andersson, J. Högström, W. Fredriksson, K. Edström, L. Nyholm, U. Jansson, Influence of deposition temperature and amorphous carbon on microstructure and oxidation resistance of magnetron sputtered nanocomposite CrC films, Applied surface science 305 (2014) 143-153.
[71] X.-L. Shang, Z.-J. Wang, Q.-F. Wu, J.-C. Wang, J.-J. Li, J.-K. Yu, Effect of Mo Addition on Corrosion Behavior of High-Entropy Alloys CoCrFeNiMo x in Aqueous Environments, Acta Metallurgica Sinica (English Letters) 32(1) (2019) 41-51.
[72] O. El-Atwani, N. Li, M. Li, A. Devaraj, J. Baldwin, M.M. Schneider, D. Sobieraj, J.S. Wróbel, D. Nguyen-Manh, S.A. Maloy, Outstanding radiation resistance of tungsten-based high-entropy alloys, Science advances 5(3) (2019) eaav2002.
[73] A. Erdoğan, S. Zeytin, Influence of Al and Ti elements on the microstructure and properties of crnifecoalxtiy heas fabricated by ECAS, (2016).
[74] Y. Zhang, T.T. Zuo, Z. Tang, M.C. Gao, K.A. Dahmen, P.K. Liaw, Z.P. Lu, Microstructures and properties of high-entropy alloys, Progress in Materials Science 61 (2014) 1-93.